Pore network model of the cathode catalyst layer of proton exchange membrane fuel cells: Analysis of water management and electrical performance

Mohamed El Hannach, Marc Prat, Joel Pauchet

Pore network model of the cathode catalyst layer of proton exchange membrane fuel cells: Analysis of water management and electrical performance

Mohamed El Hannach [a], *Marc Prat* [b,c,*], *Joël Pauchet* [a,**]

[a] *CEA, LITEN, LCPEM, F-38054 Grenoble, France*
[b] *Université de Toulouse, INPT, UPS, IMFT, Avenue Camille Soula, 31400 Toulouse, France*
[c] *CNRS, IMFT, 31400 Toulouse, France*

A B S T R A C T

A pore network modeling approach is developed to study multiphase transport phenomena inside a porous structure representative of the Cathode Catalyst Layer (CCL) of Proton Exchange Membrane Fuel Cell. A full coupling between two-phase transport, charge transport and heat transport is considered. The liquid water evaporation is also taken into account. The current density profile and the liquid water distribution and production are investigated to understand the liquid production mechanism inside the CCL. The results suggest that the wettability and the pore size distribution have an important impact on the water management inside the cathode catalyst layer and thus on the performances of the proton exchange membrane fuel cell. Simulations show also that Bruggemann correlation used in classical models does not predict correctly gas diffusion.

Keywords:
Multiphase transport
Pore network
Catalyst layer
Water management

1. Introduction

Proton exchange fuel cells are one of the promising alternatives to convert energy with high efficiency to power engines for transportation application. Recently there have been many studies conducted to improve these fuel cells. The main challenges are to reduce their cost and to increase their lifetime. The catalyst layer is one of the key components to reduce the cost of the fuel cell. According to the Department Of Energy (DOE) Hydrogen program 2010 annual progress report, the catalyst layer represents 47.6% of the cost of PEMFC stack [DOE 2009]. This component is also home to several physical phenomena that affect directly the global performance of the cell. These phenomena are mainly the electrochemical reaction, the mass transport, the charge transport, the heat transport, the water production and possibly liquid–vapor phase change.

Owing to its small thickness (less than 30 μm typically) and the nanoscale pore sizes involved, the microstructure of the CL is difficult to determine. One option used recently is to rely on three-dimensional transmission electron microscopy tomography and scanning transmission electron microscopy. For example in Ref. [1], a focused ion beam/scanning electron microscope was recently used for the reconstruction of the catalyst layer morphology. However, even if the structure of the CL begins to be better understood, it is still difficult to model it. As in many previous studies, we will adopt the widely accepted representation of the CL based on the

* *Corresponding author*. Université de Toulouse, INPT, UPS, IMFT, Avenue Camille Soula, 31400 Toulouse, France.
** *Corresponding author*.
E-mail addresses: melhannach@gmail.com (M. El Hannach), prat@imft.fr (M. Prat), joel.pauchet@cea.fr (J. Pauchet).

agglomerate approach [2–6], which considers that the porous structure of the CL is made by the staking of spherical agglomerates, composed of C/Pt particles and the ionomer (Nafion®). This approach allows studying the effect of some structural parameters such as the agglomerate size and the Nafion® film thickness [4,5].

Regarding the modeling of transport phenomena, most of the CL models are based on a macrohomogeneous approach [6–10]. This approach is more suitable for PEMFC performance models (models describing the behavior of a whole cell), but needs the knowledge of the effective properties of the CL.

Somehow surprisingly since water management is a key issue in PEMFC, few models consider the effect of liquid water inside the CCL [6,9,10]. Eikerling [9,10] developed a structure-based model of the CCL, to study the effect of the liquid and the porous media properties on the fuel cell performances. The pore size distribution and the wetting properties of the CCL are indeed important to ensure better water management. The capabilities of the model to study the effect of the structural parameters locally are however limited.

The Pore Network Modeling (PNM) approach used in the present paper is distinct from the aforementioned approaches. In particular, it presents interesting capabilities for analyzing two-phase, i.e. liquid–gas, transport phenomena inside porous media. It has been largely used in the context of soil physics or petroleum engineering and much more recently applied to study water management inside the Gas Diffusion Layer (GDL) of the PEM fuel cell [12–19]. Among other things, the PNM approach allows linking the local structural properties to the effective transport parameters of the macrohomogeneous models.

Contrary to GDLs, the pore network approach has not been fully applied to the modeling of transfers in CCL. To the best of our knowledge, one can quote only two articles aiming at developing the pore network approach of CCL, e.g [20,21]. The main objective of the present paper is therefore to fill this gap and to illustrate the interesting (we believe) capabilities of this approach. The model described in what follows is based on our previous work [20], which was restricted to the (uncoupled) modeling of liquid water migration and the modeling of gas diffusion, two important aspects for the CCL PN modeling. The objective is therefore to propose in the present paper a fully coupled 3D two-phase multi-physic pore network model of the CCL, including the main phenomena occurring in a CCL (charges transport, electrochemical reaction, liquid migration, evaporation, etc). The capabilities of the model are illustrated through a series of numerical simulations.

As in Ref. [20], the model is based on the agglomerate model, which describes the active layer as a porous medium made of agglomerates (typical size 100–1000 nm) each of them made of several C/Pt grains (typical size 30 nm). Thus within the framework of the agglomerate model, the CCL is viewed as a dual porosity medium. The "large" pores (also referred to as the "secondary" pores) correspond to the voids existing between the agglomerates whereas the small pores ("primary" pores) correspond to the pores within the agglomerates. Our model is based on a somewhat simplified representation considering the CCL as a two-phase heterogeneous system: the first phase (the pore space) corresponds to the large pores (void space between agglomerates, detailed in Section 2) whereas the second phase (the agglomerate phase) corresponds to the agglomerates (see Section 3). For simplicity, the agglomerate phase is referred to as the "solid" phase.

The oxygen reduction reaction (ORR) is supposed to occur at the surface of the agglomerates and it is described in Section 4. Results obtained with the fully coupled model are presented and discussed in Section 5.

2. PNM for two-phase transfer in the void phase

2.1. *Description of the PNM*

The secondary pores are represented with a 3D pore/throat network (see Fig. 1). As detailed in Ref. [20] the network is considered cubic with a constant lattice spacing $\delta = 150$ nm (δ is the distance between two adjacent pores). Each pore is spherical and is connected to 6 neighbor pores through 6 adjacent cylindrical throats (2 in each direction).

The diameters of the throats d_t are specified using a "pore" size distribution (PSD) of a real CCL structure. The diameter of a pore d_p is set to be higher than the largest throat connected to it $d_p = \max(d_t) + \Delta d$ where Δd is a constant parameter used to control the total porosity of the CCL.

This network is used to compute the gas phase and the liquid water transport. The gas diffusion through the Nafion® film (see section 3.1) is not considered in this model.

Determining the wettability properties of CCL is still an open problem. We assume that the CCL is a system of mixed wettability. This property is implemented using the contact angle θ (measured in liquid water). A pore or a throat is either hydrophobic ($\theta \approx 100°$–°contact angle of water on Nafion®) or hydrophilic ($\theta \approx 65°$–°contact angle of water on the carbon used in the CCL considered as reference for this work). The percentage of hydrophilic pores and throats (or equivalently

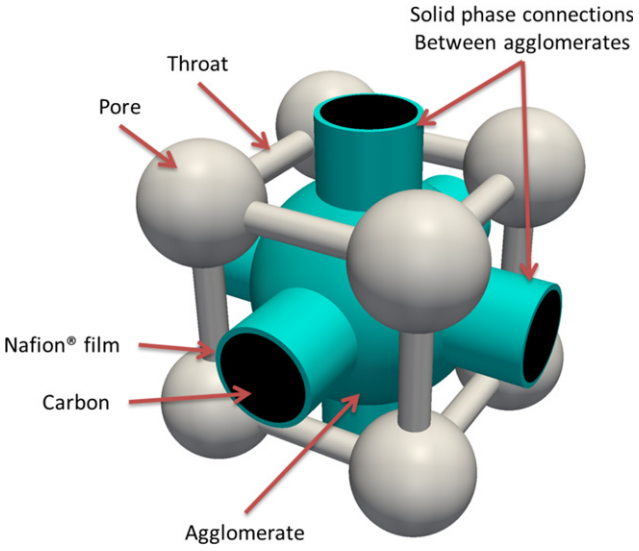

Fig. 1 – Schematic of the pore network and the solid phase network elements and their relative position.

the probability for a pore or a throat to be hydrophilic) is an input parameter of the model, see Ref. [20] for more details. This allows considering relatively easily various hypotheses as regards the wettability of CCL.

2.2. Liquid water transport

Inside the CCL pores the liquid water invasion is mainly controlled by the capillary forces, see Ref. [20] for more information. For example the liquid water presents in a given pore (respectively a throat) will invade one of the adjacent throats (respectively a pore) depending on the value of the invasion capillary pressure threshold associated with each element (pore or throat). This pressure represents the minimum pressure difference between the liquid phase and the gas phase required for the liquid to invade an adjacent element (pore or throat). The higher this pressure, the harder to invade the corresponding pore network elements. For each pore and throat, a capillary pressure threshold is computed using the following formula, [20]:

$$p_{\mathrm{cth}} = -\frac{4\gamma\cos\theta}{d_n} \tag{1}$$

where γ is the surface tension; $d_n = d_t$ for a throat whereas d_n depends on the wetting properties for a pore and is computed as follows:

$$\begin{cases} d_n = d_p & \text{if } \theta > 90^\circ \\ d_n = d_p + \sum_{i=1}^{n} b_i k_i d_{t,i} & \text{if } \theta < 90^\circ \end{cases} \tag{2}$$

The use of distinct expressions for the hydrophilic case ($\theta < 90^\circ$) and the hydrophobic case ($\theta > 90^\circ$) is due to the nature of the invasion process in the hydrophilic network. As discussed in more detail in Ref. [20], the invasion of a hydrophilic pore depends on the status (invaded by liquid or not) of the adjacent throats, because in this case the invasion process is a cooperative process (i.e. depends on the menisci growth in adjacent throats and not only on the growth of the meniscus in the pore). The simplified approach represented by the second line of Eq. (2) and used here to take into account the cooperative effect was proposed by Blunt [22]. In Eq. (2), n represents the number of adjacent throats filled with air. k_i are random numbers generated between 0 and 1. The parameters b_i are expressed as a function of the (arithmetic) average diameter of all the adjacent throats $<d_t>$: $b_1 = 0$, $b_2 = 5/<d_t>$, $b_3 = 10/<d_t>$, $b_4 = 50/<d_t>$, $b_5 = 100/<d_t>$.

The invasion algorithm used to simulate the liquid water invasion inside the pore network can be summarized as follows:

- The pore or the throat with the smallest capillary pressure threshold is invaded first.
- Only one (interfacial) element is invaded at the boundary of each liquid cluster in each time step (viscous forces are negligible compared to the capillary forces).
- The time step is chosen so that only one interfacial element is fully invaded by liquid water.

This part of the model is detailed in Ref. [20] and therefore the details are not repeated here. In Ref. [20], two algorithms, referred to as the sequential and kinetic algorithms respectively, were presented and discussed. The algorithm used here is a kinetic algorithm, see again Ref. [20] for more details.

2.3. Gas diffusion

The gas transport inside the CCL porosity (pore network) is described by a diffusion model based on Stefan Maxwell equations as proposed in Ref. [20]. For a gas component "i" (O_2 or H_2O) the molar fraction gradient is expressed as functions of the diffusion coefficients D_j (where "j" denotes O_2, H_2O and N_2) and the molar fluxes of different species as follows [23]:

$$c\nabla x_i = \sum_j \left(\frac{x_i J_j}{D_j} - \frac{x_j J_i}{D_i}\right) \tag{3}$$

where c (mol m^{-3}) is the total gas phase concentration; $x_i = c_i/c$ is the molar fraction of the gas component "i" (O_2 or H_2O); J (mol m^{-2} s^{-1}) is the molar flux.

The gas total pressure gradient is given by the following equation [23]:

$$\nabla p = -\frac{32\mu}{cd^2(1+Knp)}\frac{\sum_j \left(M_j^{1/2} J_j\right)}{\sum_j \left(x_j M_j^{1/2}\right)} \tag{4}$$

where Knp is a parameter depending on the Knudsen number Kn and on the molar mass of the gas components [23]:

$$Knp = \frac{128}{3\pi}\frac{\left(\sum_j (x_j M_j)\right)^{1/2}}{\sum_j \left(x_j M_j^{1/2}\right)} Kn \tag{5}$$

In this work we suppose that N_2 is stagnant ($J_{N2} = 0$ mol m^{-2} s^{-1}). Inside the (secondary) pores of the CCL (10–100 nm), the Knudsen effect is important and therefore included in the model using the Knudsen diffusion coefficient $D_{k,i}$ defined as follows [23]:

$$D_{k,i} = \frac{d}{3}\left(\frac{8R_g T}{\pi M_i}\right)^{1/2} \tag{6}$$

The diffusion coefficient in Eq. (11) is:

$$D_i = \left(\frac{1}{D_b} + \frac{1}{D_{k,i}}\right)^{-1} \tag{7}$$

where D_b is the binary diffusion coefficient.

These equations are used to compute the gas diffusion conductance between two adjacent gaseous or partly gaseous pores (see Ref. [20] for more details). The presence of liquid water inside the pores affects the gas transport, so the gas diffusion conductance is corrected accordingly. As sketched in Fig. 2, the cross section area is modified differently depending on the wettability properties. In the hydrophilic case the liquid water forms a film around the inner wall of the pore. In the hydrophobic case the liquid water is distributed inside the pore as spherical droplets. Thus, for the same amount of liquid water, the gas flow cross-section area is smaller when the pores are hydrophobic. The correction factors used to account for the liquid water distribution inside the pores and the throats are summarized in Table 1. For example, in the

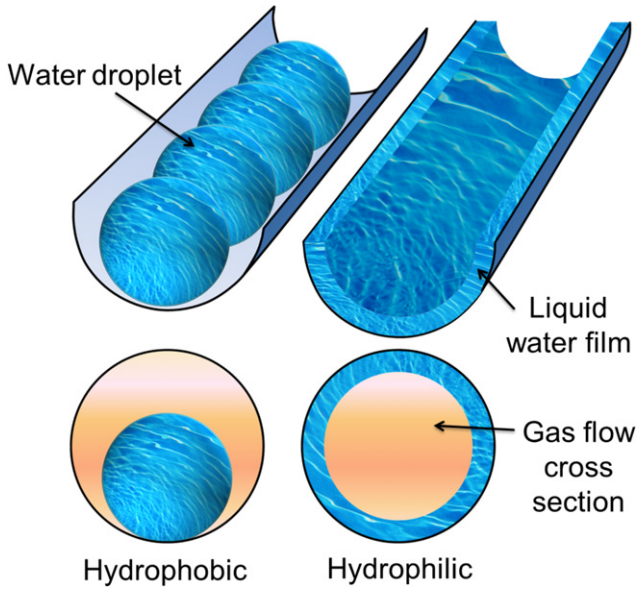

Fig. 2 – Schematic of the effect of the liquid water on the gas transport cross section area in a hydrophobic (left) and a hydrophilic (right) pore network element.

case of a hydrophobic throat, the diffusion conductance will be equal to 0 when the liquid water saturation s_l inside the throat (s_l is equal to the volume of the liquid water divided by the total volume of the throat) is equal or greater than 2/3, while in the hydrophilic throat the correction function is different from 0 as long as $s_l < 1$. Hence the correction factors presented in Table 1 are used to correct the cross section area for the gas phase depending on the amount of liquid water present inside the pore/throat and how it is distributed. More details about the diffusion model development and validation can be found in Ref. [20].

2.4. *Evaporation*

The water is supposed to be produced in liquid phase at the surface of the agglomerates. Evaporation is therefore possible depending on the temperature and the water vapor partial pressure conditions in adjacent pores. The evaporation can occur at two different scales. The first one corresponds to the agglomerate surface, when water enters the pores. When the evaporation rate at this level is lower than the water production rate, liquid water can fill the pores and invades the porous structure of the CCL creating liquid water clusters. The second scale of the evaporation process corresponds to the boundary of these water clusters. At this larger scale, the evaporation reduces or even sets to zero the water cluster growing rate.

The evaporation rate is computed using the following formula originally derived by Schrage [24] based on kinetic theory:

$$J_{ev} = \frac{2\sigma_{acc}}{2-\sigma_{acc}}\left(\frac{1}{2\pi RTM_{H2O}}\right)^{1/2}(p_{lv} - p_{H2O}) \quad (8)$$

where p_{lv} is the equilibrium water vapor partial pressure and $p_{H2O} = x_{H2O}p_g$ is the water vapor pressure around an agglomerate or at the liquid/gas interface of a liquid water cluster (it depends on the scale the evaporation is computed). p_g is the total pressure of the gas phase, σ_{acc} is an accommodation coefficient. Eq. (8) is used to link the evaporation rate to the difference between the equilibrium water vapor pressure and the water vapor pressure at the liquid/gas phase interface (see Ref. [24] for more details).

The evaporation process depends on meniscus curvature via the modification of water vapor equilibrium partial pressure with the meniscus curvature, which in turn depends on the wetting properties and the pore diameter. This is taken into account using the Kelvin equation [25]:

$$p_{lv}(T, d_p, \theta) = p_{lv}(T)\exp\left(-\frac{4\gamma M_{H2O}\cos\theta}{\rho_{H2O}R_g T d_p}\right) \quad (9)$$

For example, this equation allows to take into account that p_{lv} (and thus the evaporation rate) is lower in the small hydrophilic pores rather than in the large hydrophilic pores.

Table 1 – Corrections of the diffusion conductance as function of the wettability and the liquid water saturation inside the pores and the throats.

	Pore	Throat
Hydrophilic	$(1 - s_l)^{2/3}$	$(1 - s_l)$
Hydrophobic	$1 - (s_l)^{2/3}$	$\max(0; 1 - 3/2s_l)$

3. PNM for charge and heat transfer in the solid phase

3.1. *Description of the PNM*

For the solid phase, a cubic agglomerate network similar to the pore network is constructed with agglomerates and cylindrical bonds between two neighbor agglomerates. Each agglomerate is connected to 6 other agglomerates, distant with the same lattice spacing δ. The bonds between two adjacent agglomerates are called connections to distinguish them from the void phase bonds which are called throats (see Fig. 1). In reality the shape of the agglomerates is not spherical but is represented in the model as an equivalent sphere (sphere of same volume as the agglomerate).

For the solid phase network, the geometric properties specified in the model are the surface area of the agglomerate φ_{agg} and the thickness of the Nafion® film e_N surrounding each agglomerate. The active area of the CCL is a parameter measured to estimate the efficiency of the CCL structure regarding the electrochemical activity. This parameter is divided by the number of agglomerates to determine φ_{agg} which is considered the same for all the agglomerates. The diameters of the solid bonds are calculated depending on the diameters of the surrounding pores (see Eq. (10) for the mathematical expressions).

The heat and the charge transports are computed over the agglomerate network.

3.2. Charge transport

To compute the charge transport, the electronic and protonic potentials ψ_{e-} and ψ_{H+} are computed at each agglomerate. The connection between two agglomerates is supposed to be cylindrical, with a carbon core (for electron transport) and a thin Nafion® film (for proton transport) covering it. The thickness of the Nafion® film is an input parameter of the model. The diameter of the connection d_{con} is calculated as a function of the surrounding pores diameters.

$$d_{con} = \left(4\frac{\delta^2}{\pi} - \sum_i \frac{d_{p,i}^2}{4}\right)^{1/2} \tag{10}$$

This diameter is equal to the diameter of the disk that has the same area as the cross section area between two adjacent agglomerates. This area is delimited mainly by the 4 pores surrounding a solid phase connection (see Fig. 1). So when the surrounding pores have large diameters, the diameter of the connection is small.

The electron conductivity is supposed to be constant. However the proton conductivity is calculated as a function of the local relative humidity. The dependence of the proton conductivity on the temperature and the relative humidity was taken from the measurements presented in Ref. [26] on adsorbed Nafion® film. An interpolation function was used to incorporate the measurement data into the model:

$$\sigma_{H+} = 100 \times \exp\left((15.036 \times a_{H2O} - 15.811)\frac{1000}{T} + (-30.726 \times a_{H2O} + 30.481)\right) \tag{11}$$

The current densities of the electrons and the protons transport are defined as follows:

$$\begin{cases} j_{e-} = -\sigma_{e-}\nabla\psi_{e-} \\ j_{H+} = -\sigma_{H+}\nabla\psi_{H+} \end{cases} \tag{12}$$

For a given agglomerate, the charge balance is expressed as follows:

$$\begin{cases} \sum_i \left(\phi_{e-,i} j_{e-,i}\right) = -\phi_{agg} j_{orr} \\ \sum_i \left(\phi_{H+,i} j_{H+,i}\right) = \phi_{agg} j_{orr} \end{cases} \tag{13}$$

where "i" denotes the adjacent agglomerates, j_{orr} is the current density produced by the ORR (A m^{-2}); $\varphi_{e-,i}$ and $\varphi_{H+,i}$ represent the cross section areas of the electrons and the protons conducting phases (respectively carbon and the Nafion® film surrounding it). They are calculated as function of the connection diameter and the Nafion® film thickness:

$$\begin{cases} \phi_{e-} = (\pi/4)(d_{con} - 2e_N)^2 \\ \phi_{H+} = (\pi/4)\left(d_{con}^2 - (d_{con} - 2e_N)^2\right) \end{cases} \tag{14}$$

3.3. Heat transport

Inside the CCL, the heat is mainly generated by the ORR and the Joule effect due to charge transport resistance of the conductive materials.

The heat balance at each node of the agglomerate network is expressed as:

$$\sum_i \left(\varphi_{T,i}(-\lambda_T \nabla T)\right) = W_{joule} + W_{overpotential} + W_{ORR} \tag{15}$$

where $\varphi_{T,i}$ is the cross section area of the connection between two adjacent agglomerates:

$$\phi_T = \frac{\pi}{4} d_{con}^2 \tag{16}$$

The source terms are given by the following equations:

$$W_{joule} = \frac{\phi_{e-}}{\delta}\frac{(j_{e-})^2}{\sigma_{e-}} + \frac{\phi_{H+}}{\delta}\frac{(j_{H+})^2}{\sigma_{H+}} \tag{17}$$

$$W_{overpotential} = \phi_{agg} j_{orr} \eta \tag{18}$$

$$W_{ORR} = \phi_{agg} j_{orr} \frac{T\Delta S_{orr}}{4F} \tag{19}$$

Note that the heat transfer associated with the evaporation process is negligible compared to the other heat sources, thus for simplification it is not considered in this model.

4. PNM of a CCL with coupled transfers

4.1. Electrochemical reaction

The transport phenomena in the two networks are related mainly by the ORR which is supposed to occur at the surface of the agglomerates. The ORR is described using the Butler–Volmer equation [27]:

$$j_{orr} = j^0 (a_{O2})^{1/4} (a_{H2O})^{1/2} \left[\exp\left(2\frac{\alpha F}{RT}\eta\right) - \exp\left(-2\frac{(1-\alpha)F}{RT}\eta\right)\right] \tag{20}$$

where R is the gas constant and F is the Faraday constant. The over potential η is calculated as functions of the electronic and the protonic potentials:

$$\eta = \psi_{e-} - \psi_{H+} - E^0 \tag{21}$$

The current density is calculated at each agglomerate (=nodes of the agglomerate network). In the 3D networks, each agglomerate (represented with a sphere) is surrounded by 8 pores (see Fig. 1). The activities of oxygen and water are computed from the partial pressure inside the pores surrounding the agglomerate.

$$\begin{aligned} a_{O2} &= \frac{\sum_i a_{O2,i}}{\text{number of surrounding pores}} \\ a_{H2O} &= \frac{\sum_i a_{H2O,i}}{\text{number of surrounding pores}} \end{aligned} \tag{22}$$

where $a_{O2,i}$ and $a_{H2O,i}$ represent the activities of oxygen and water inside the pore "i".

The flow rates of oxygen consumption and water production are calculated for each agglomerate using j_{orr} and they are distributed equally over the surrounding 8 pores (see again Ref. [20] for more details). The solid phase and void phase networks interact with each other via the activities of oxygen and water (Eq. (22)) and their consumption/production rates.

4.2. *Boundary conditions*

The boundary conditions are summarized in Fig. 3. Most of the boundary conditions are applied at the CCL/PEM and the CCL/GDL interfaces. The pressure and the temperature operating conditions are introduced as Neumann boundary conditions to account for the heat transport inside the fuel cell components in the cathode and the anode sides, and for the gas diffusion inside the cathode GDL.

The heat fluxes $\omega_{CCL/GDL}$ and $\omega_{CCL/PEM}$ at the CCL/GDL and the CCL/PEM interfaces respectively are expressed as follows:

$$\begin{aligned}\omega_{CCL/GDL} &= -\lambda'_{Teq,GDL}\left(T_{CCL/GDL} - T_{Channel}\right)\\ \omega_{CCL/PEM} &= -\lambda'_{Teq,PEM}\left(T_{CCL/PEM} - T_{Channel}\right)\end{aligned} \tag{23}$$

where the parameters $\lambda'_{Teq,GDL}$ (W K^{-1} m^{-2}) and $\lambda'_{Teq,PEM}$ (W K^{-1} m^{-2}) represent the equivalent thermal conductivities of the cathode GDL and the assembly (PEM + anode CL + anode GDL) respectively. These parameters are expressed as follows:

$$\begin{aligned}\lambda'_{Teq,GDL} &= \frac{\lambda_{T,GDL}}{e_{GDL}}\\ \lambda'_{Teq,PEM} &= \left(\frac{e_{PEM}}{\lambda_{T,PEM}} + \frac{e_{ACL}}{\lambda_{T,ACL}} + \frac{e_{GDL}}{\lambda_{T,GDL}}\right)^{-1}\end{aligned} \tag{24}$$

where e_{PEM}, e_{GDL} and e_{ACL} are the thicknesses of the PEM the GDL and the anode CL respectively. The values of thermal conductivities of the fuel cell components are taken from Ref. [32].

The gas diffusion from the cathode channel through the cathode GDL is represented using the following boundary condition:

$$J_{CCL/GDL} = -\frac{D_{GDL}}{e_{GDL}}\left(c_{CCL} - c_{Channel}\right) \tag{25}$$

where D_{GDL} is the diffusion coefficient inside the GDL, and $c_{Channel}$ is the molar concentration of the gas phase component (O_2 or H_2O) at the cathode channel.

Periodic conditions are considered in the in-plane directions.

4.3. *Method of solution*

The above formulation of the transport phenomena (gas diffusion, charge transport and heat transport) leads to the consideration of 4 linear systems: 1 for gas transport (derived from Eq. (3)), 2 for charge transport (Eq. (13)) and 1 for heat transfer (Eq. (15)). The unknowns of these systems are: oxygen and water vapor concentrations inside the pores, electronic potential, protonic potential and temperature in the agglomerates. Each system is solved in stationary state using the Generalized Minimal RESidual method (GMRES) [29]. The solver is based on iterative method where the solution is obtained when the variation of each unknown does not exceed a given acceptable error between two successive iterations.

The systems are coupled together with the Butler–Volmer equation, which is used to compute j_{orr} at every agglomerate. So a second convergence criteria is added and it is related to j_{orr}. Indeed, after solving each system the values of j_{orr} are updated and the final solution is obtained when the variation of j_{orr} is less than 0.01 A m^{-2} (the minimum values of j_{orr} are around -10 A m^{-2}). In the first time step, few tens of iterations are necessary, and only few iterations are enough for the rest of the simulation.

The evaporation flow rates are also computed at each step. If liquid water is produced the invasion algorithm is used to calculate the liquid water distribution inside the CCL. The diffusion conductances are updated regarding the new liquid distribution and the linear systems are solved again. This process is summarized in Fig. 4.

Using a single Intel® Nehalem 64 bits 2.27 GHz CPU the simulation time varies between two weeks and more than one month. The throat and pore sizes are randomly distributed according to the PSD. A given specification of throat and pore sizes is called a realization of network. The simulations were repeated for several realizations of network to be sure that the global tendencies are independent of the particular realization considered.

The purpose of this work is to study in detail local transport phenomena in the CCL, so the simulations were conducted in one stationary point of the polarization curve. Unfortunately one simulation can take around a month so we didn't generate enough data for a polarization curve but we focused on the effect of different parameters in one point.

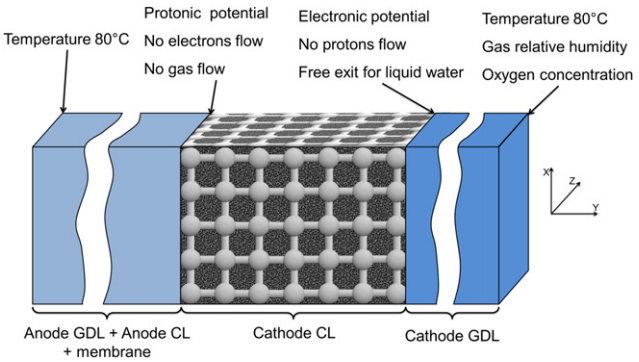

Fig. 3 – Summary of boundary conditions.

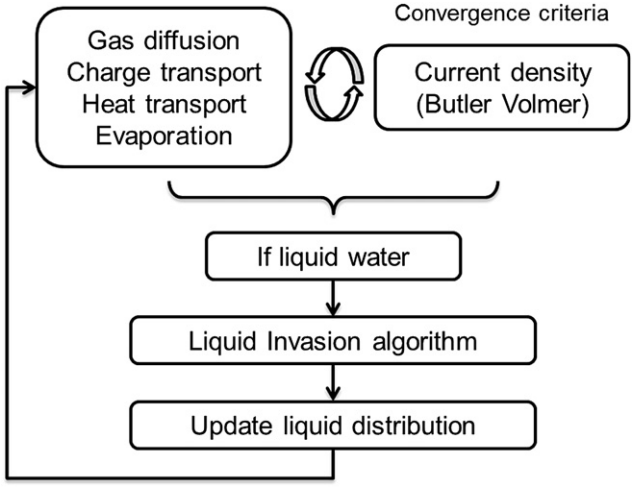

Fig. 4 – Summary of the method of solution.

5. First analysis with the coupled CCL PNM

The simulations were made using a 3D network of size 10 × 100 × 10 (number of pores in the X, Y and Z directions of a Cartesian coordinate system, respectively). The Y direction is the through plane direction, i.e. along the thickness of the CCL between the membrane and the GDL (see Fig. 3). The number of the pores in the X and the Z directions were specified so as to have computational times not exceeding one month. In this work the modeled CCL has a thickness equal to 15 μm. The Gas inside the cathode channel is supposed to be highly humidified air (95%), and the operating temperature is 80 °C. The main parameters are summarized in Table 2. The aim of simulations is to illustrate the capabilities of the CCL PN model. In particular, determining whether the CCL is dry (liquid water within the agglomerates only), partly invaded by liquid water or flooded is of a primary interest as regards the water management issue and the operation of PEMFCs.

Two pore size distributions are considered. They are referred to as "PSD 1" [1] and "PSD 2" [11]. As shown in Fig. 5, the main difference between the two PSDs is that "PSD 1" has more large pores than "PSD 2". As explained in Section 2, the pore network is made from cylindrical throats and spherical pores. The diameters of the throats are generated according to the PSD measurement. However, the pore diameters are generated depending on the diameters of the adjacent throats and the total porosity of the CCL structure.

In the following subsections, the main output parameters obtained using the PSD 1 and 20% hydrophilic network are presented and discussed. The effect of the PSD and the wettability on the gas diffusion coefficient is also explored.

Table 2 – Summary of the main model parameters.

Parameter	Value
Porosity	$\varepsilon = 39\%$
Specific surface area	5×10^5 m^{-1} [30,31]
Exchange current density	$j^0 = 1.8 \times 10^{-2}$ A m^{-2} [30]
Electronic potential at CCL/GDL	$\psi_{e^-} = 0.68$ V
Protonic potential at CCL/GDL	$\psi_{H^+} = -0.165$ V
Hydrophilic contact angle	65°
Hydrophobic contact angle	100°
Binary diffusion coefficient	$D_b = 2.02 \times 10^{-5}$ m^2 s^{-1}
Nafion® film thickness	$e_N = 5$ nm
Electric conductivity of carbon	$\sigma_{e^-} = 1000$ S m^{-1}
Thermal conductivity of carbon	$\lambda_T = 0.5$ W m^{-1} K^{-1} [32]
Thermal conductivity of the ACL	$\lambda_{T,ACL} = 0.27$ W m^{-1} K^{-1} [32]
Thermal conductivity of the PEM	$\lambda_{T,PEM} = 0.12$ W m^{-1} K^{-1} [32]
Thermal conductivity of the GDL	$\lambda_T = 1.7$ W m^{-1} K^{-1} [32]
Gas temperature in the channels	$T_{Channel} = 353$ K
Gas relative humidity in the cathode channel	95%
Oxygen concentration at the cathode	$c_{O2,Channel} = 7.35$ mol m^{-3}
Total gas pressure in the cathode channel	1.5×10^5 Pa
ACL thickness	$e_{ACL} = 10$ μm
PEM thickness	$e_{PEM} = 50$ μm
GDL thickness	$e_{GDL} = 300$ μm

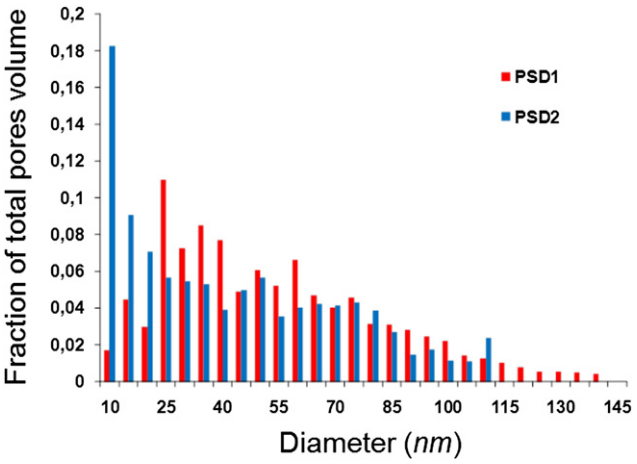

Fig. 5 – The two PSDs used in the simulations. The total porosity obtained with both PSDs is 39%.

5.1. Current density

One of the main parameters used to evaluate the CCL performance is the total current density I_{CCL} (mA/cm^2), which represents the total current produced by the CCL per unit area of the CCL. The total current density is calculated by adding the current densities produced by all the agglomerates in the CCL. The value of I_{CCL} is determined when the simulation reaches a stable state, which is obtained when the liquid water saturation inside the CCL does not increase anymore. This state means that either all the produced liquid water evaporates before reaching the CCL/GDL interface or finds a preferential pathway in liquid phase up to the CCL/GDL interface. The total liquid water saturation, obtained over the whole CCL when the stable state is reached is also an output parameter. A drop of I_{CCL} is observed from 890 mA/cm^2 to 574 mA/cm^2 when the total liquid water saturation rises from 0 to 0.59 (Fig. 8). The presence of liquid water has an important effect on the performances of the CCL, but doesn't always lead to a total flooding.

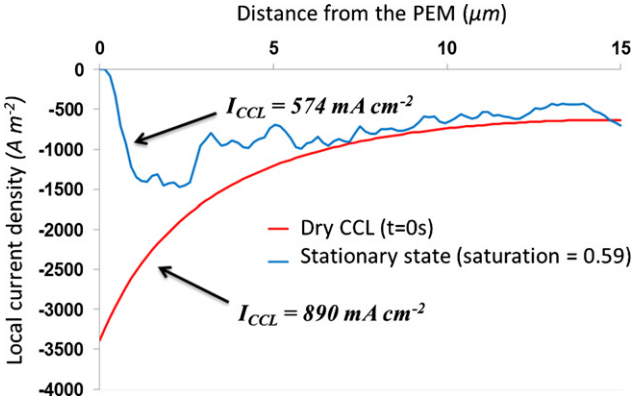

Fig. 6 – Local current density profile through the thickness of the CCL obtained using PSD 1 and a 20% hydrophilic network.

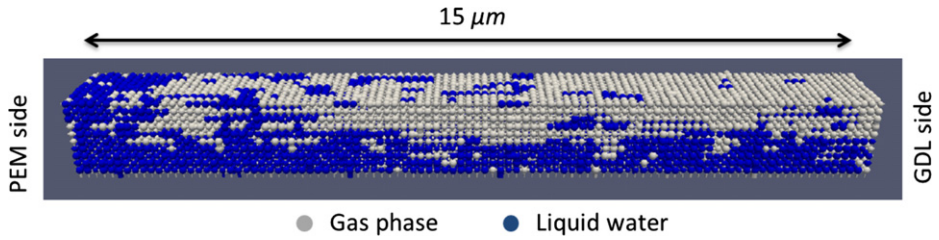

Fig. 7 – Liquid water distribution inside the CCL pore network; liquid phase in blue, gas phase in gray. 20% hydrophilic network ($s_l = 0.59$, $I_{CCL} = 574$ mA cm^{-2}). (For interpretation of the references to colour in this figure legend, the reader is referred to the web version of this article.)

The profile of the local current density, expressed per unit of area of the agglomerate active surface, is used to evaluate the effect of water distribution on the CCL performances through its thickness. The profile of the local current density shows that the CCL is more active at PEM side. Almost 50% of the current is generated in the third of the CCL which is the closest to the PEM (see results for dry CCL in Fig. 6). This results from the proton transport limitation, which is higher than the oxygen transport limitation. At the stationary state, a decrease of the electrochemical activity is observed all along the CCL thickness. The CCL/PEM interface seems to be flooded since no electrochemical activity is recorded.

5.2. *Liquid distribution*

The distribution of liquid water inside the 3D pore network is presented in Fig. 7. More water presence is observed near the PEM. More details about the liquid distribution can be obtained from the liquid water saturation profile calculated along the thickness of the CCL. The in-plane slice average liquid water saturations are calculated over the pores and the throats situated in the same XZ planes along the thickness of the CCL. The saturation profile corresponds to the evolution of the slice average saturation along the thickness of the CCL.

For the first time steps of the simulation, there is more liquid water near the PEM and near the GDL than in the middle of the CCL (Fig. 8). The total liquid water saturation rises keeping almost the same profile. However, the liquid presence near the PEM increases rapidly and at the final state of the simulation, the CCL/PEM interface is almost completely flooded (Fig. 8). This observation is in agreement with the results shown in Fig. 6, where the local current density is near 0 at the CCL/PEM interface.

Productive agglomerates are the agglomerates that produce water in liquid phase, which depends on the difference between water production with the ORR and the evaporation flow rates. Nonproductive agglomerate can be either a flooded agglomerate, where no more oxygen reaches the catalyst, or an active agglomerate that produces water but in vapor phase. A profile of the percentage of the productive agglomerates is shown in Fig. 9. This parameter allows investigating how liquid water is produced through the thickness of the CCL.

The first productive agglomerates are located near the GDL (Fig. 9, t = 0 s). During the simulation more agglomerates are becoming productive inside the CCL. The percentage of productive agglomerates rises from 0 to almost 60% near the PEM in the first 30 s of the simulation (Fig. 9). This high production explains the increase of the liquid water saturation near the PEM, which leads to the flooding of this zone of the CCL.

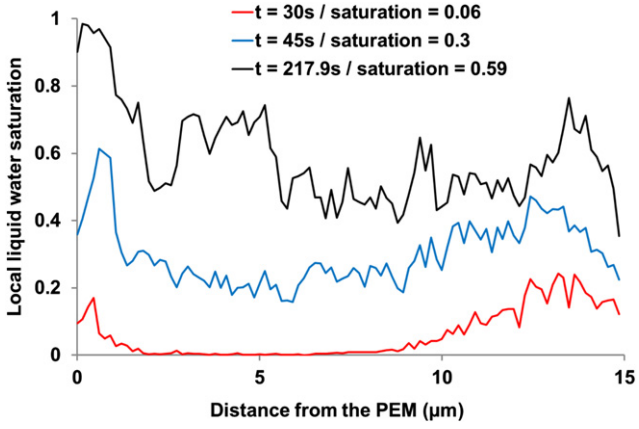

Fig. 8 – Liquid water saturation profile through the thickness of the CCL for a 20% hydrophilic CCL at different time steps.

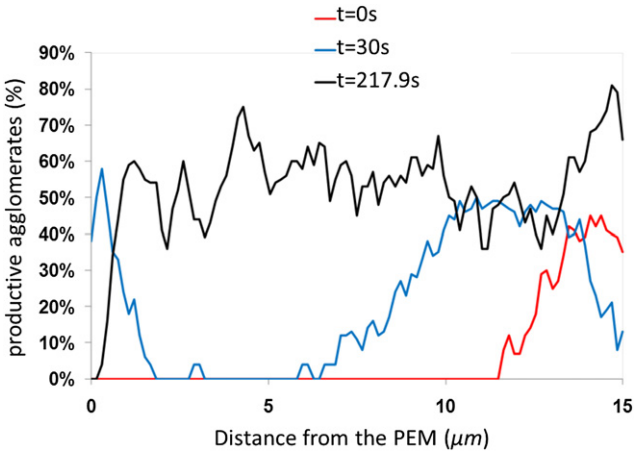

Fig. 9 – Profile of the percentage of the productive agglomerates through the thickness of the CCL. The results are obtained using PSD 1 and a 20% hydrophilic.

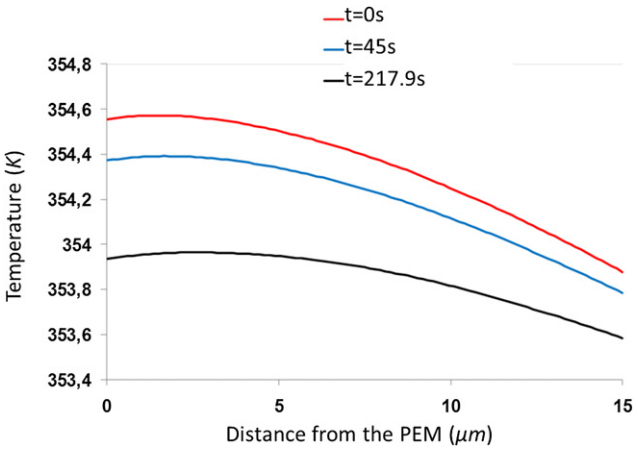

Fig. 10 – Temperature profile through the thickness of the CCL at different time steps, obtained using PSD 1 and a 20% hydrophilic network.

5.3. *Liquid water production mechanism*

The relative humidity and the temperature local conditions are very important to understand how liquid water is produced through the thickness of the CCL. Fig. 10 shows the temperature profile for different time steps. In general the temperature is decreasing during the simulation. This is mainly due to the decrease of the electrochemical activity because of the flooding of certain agglomerates. The results also show that the temperature is relatively low near the GDL, since this zone is less active than near the PEM. With the relative humidity being almost the same in the first time step and across all the CCL thickness (water vapor concentration gradient between the PEM and the GDL is 0.35 mol/m^3 with higher concentration near the PEM) the lower temperature near the GDL leads to lower evaporation rates, and thus more liquid water production. This explains the distribution of the productive agglomerates observed in Fig. 9 at the first time step.

With more liquid presence near the GDL the water vapor evacuation from the CCL with diffusion mechanism becomes less efficient. This leads to an increase of the water vapor presence near the PEM (most active zone). The water vapor concentration gradient rises to around 0.60 mol/m^3. The difference is small but sufficient to decrease evaporation rates near the PEM. Once liquid water is produced near the PEM the relative humidity quickly increases and more agglomerates become productive. Liquid water presence inside the CCL increases until the liquid clusters find a pathway, depending on the capillary forces, that allows liquid water to exit the CCL at the CCL/GDL interface.

This analysis shows that the structural properties of the CCL (pore size, wettability) should be optimized to avoid the liquid production near the GDL and to allow better evacuation of water, liquid and vapor, away from the CCL/PEM interface especially when the CCL is operating in a proton limitation scenario.

5.4. *Gas diffusion*

The global oxygen diffusion coefficient is a parameter calculated by the model to estimate the oxygen diffusion over the whole CCL thickness. This coefficient is computed using the following formula:

$$Q_{O2} = AD_{CL,O2}\left(\frac{\Delta x_{O2}}{L}\right) \tag{26}$$

where Δx_{O2} is the oxygen molar fraction difference applied across the thickness of the CCL, Q_{O2} is the total oxygen flow rate across the CCL thickness, A is the cross section area of the CCL and L is the thickness of the CCL.

$D_{CL,O2}$ is mainly affected by the liquid water pore occupancy and the pore size distribution. Usually, this parameter is used in the performance models to represent the CL resistance to the gas transport. In the performance models all the fuel cell components are included and the simulations are typically performed to study the effect of the operating conditions (Temperature, pressure, humidity…) on the total current density produced by the fuel cell. So it is very important to represent accurately the transport phenomena in each component of the fuel cell, especially the CCL.

A common way to calculate this coefficient is to use the Bruggeman correlation [28], which uses the (large pore) porosity as a parameter to evaluate the diffusion coefficient for the porous medium from the free fluid diffusion coefficient $D_{CL,O2} = \varepsilon^{2/3} D_{O2}$. As shown below, this approach is not accurate especially to characterize porous structures like the CCL.

We have computed $D_{CL,O2}$ for two dry networks (free of liquid water in the large pore network) generated using the two PSDs. The total porosity of both networks is $\varepsilon = 39\%$. The simulations results are:

- $D_{CL,O2} = 8.8 \times 10^{-7}$ m^2 s^{-1} for "PSD 1",
- $D_{CL,O2} = 2.1 \times 10^{-7}$ m^2 s^{-1} for "PSD 2".

It is obvious that using Bruggeman correlation gives the same value for both PSDs. This simple example thus shows that the porosity is not sufficient to characterize the effect of CCL microstructure on gas transport.

Bruggeman like correlation is generally also used to correct the diffusion coefficient depending on the value of liquid water saturation ($D(1 - s_l)^{2/3}$). As can be seen from Fig. 11 (which represents the evolution of the diffusion coefficient while the network is invaded with liquid water), this type of correlation is not adapted to represent our results. This correlation could work only for some limited cases. For instance, the results plotted in Fig. 11 show that the oxygen diffusion coefficient dependence on the liquid water saturation can be represented to some extent using the formula $D(1 - s_l)^{2/3}$ in the case of the 80% hydrophilic network only.

For low saturation level, the liquid water can fill only partially the pores, which does not affect a lot the gas diffusion. As shown in Fig. 11, the diffusion coefficient decreases quickly in the case of the 10% hydrophilic network. At this point, the liquid water clusters begin to impede significantly the gas transport. Fig. 11 also shows that the gas diffusion is a lot better for the highly hydrophilic network (80%) than with the 50% and the 10% hydrophilic networks. This may suggest the existence of a preferential liquid water pathway for the 80% hydrophilic network.

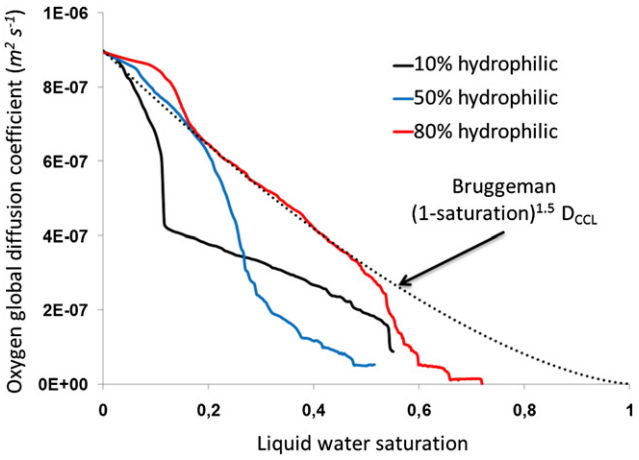

Fig. 11 – Effect of liquid water saturation on the global oxygen diffusion coefficient. Comparison with Bruggeman correlation.

More detailed study of the effect of the mixed wettability on the water management will be presented in a future work.

6. Conclusion

A multiphase three dimensional dual Pore Network Model of the CCL was presented. A detailed description of the model was provided, with particular emphasis on integrating into the model the different transport phenomena encountered in a CCL and the electrochemical reaction. In particular, the model can simulate the invasion by the liquid water of the inter agglomerates pore network when evaporation is not sufficient to evacuate the water produced as a result of the electrochemical reaction. The model also allows studying the impact of different wettability conditions (purely hydrophilic, purely hydrophobic and all intermediate cases of mixed wettability).

As illustrated through a series of numerical simulations, the model allows studying the effect of the structural properties of the CCL on the water management and the global performances. The simulations indicate that the knowledge of the local properties at the pores scale, such as the PSD and the wettability properties, is essential to determine correctly the performance of the CCL under given operating conditions.

The model predicts higher water production rate near the membrane. The liquid water appears first near the GDL due to the local temperature and relative humidity conditions. Once the liquid water is present inside the CCL the flooding is mainly observed near the membrane. The model shows the limitation of the Bruggeman correction to predict the effect of the PSD and the liquid water distribution on the gas diffusion.

Global parameters frequently used in macroscale models, such as the porosity and the overall liquid water saturation, are not sufficient to describe the CCL behavior. This model can also allow the study of the effect of other structural parameters, such as the Nafion® film thickness around the agglomerates and the CCL thickness for instance. This study thus highlights the capabilities of the proposed model and opens up the route for much more comprehensive simulation studies of CCL.

Acknowledgement

This work was partially performed in the frame of the European Project PEMICAN. The financial support of the FCH-JU Framework Program (Grant Agreement 256798), INPT and CEA is gratefully acknowledged.

Nomenclature

Latin symbols

a	water or oxygen activity
c	concentration (mol m^{-3})
d	diameter (m)
D	gas diffusion coefficient (m^2 s^{-1})
D_{CL}	global diffusion coefficient (m^2 s^{-1})
E^0	equilibrium potential (V)
e_N	Nafion® film thickness
I_{CCL}	total current density (mA cm^{-2})
j^0	exchange current density (A m^{-2})
j_{orr}	current density produced by the ORR (A m^{-2})
j	current density (A m^{-2})
J	molar flow rate (mol m^{-2} s^{-1})
Kn	Knudsen number
M	molar mass (kg mol^{-1})
p	pressure (Pa)
ΔS_{orr}	ORR entropy (J mol K^{-1})
s_l	liquid water saturation
T	temperature (K)
U	electric potential at the CCL/GDL interface (V)
W	heat production/consumption rate (J s^{-1})
x	molar fraction in gas phase

Greek symbols

α	transfer coefficient
γ	surface tension (N m^{-1})
η	over potential (V)
ε	porosity
θ	contact angle
λ_T	thermal conductivity (W K^{-1} m^{-1})
μ	gas viscosity (m s^{-1})
ρ	mass density (kg m^{-3})
σ_{acc}	accommodation coefficient
σ	charge conductivity (S m^{-1})
φ	surface area, cross section area (m^2)
ψ	potential (V)
ω	heat flux (J m^{-2} s^{-1})

Subscript

agg	related to the agglomerate
b	binary diffusion coefficient
cth	capillary threshold pressure
ev	evaporation flow rate
e–	related to electrons transport

H+	related to protons transport
H2O	water
k	Knudsen diffusion coefficient
lv	liquid/vapor equilibrium
N2	nitrogen
O2	oxygen
p	pore
t	throat

REFERENCES

[1] Ziegler C, Thiele S, Zengerle R. Direct three-dimensional reconstruction of a nanoporous catalyst layer for a polymer electrolyte fuel cell. J Power Sources 2011;196:2094–7.

[2] Secanell M, Carnes B, Suleman A, Djilali N. Numerical optimization of proton exchange membrane fuel cell cathodes. Electrochim Acta 2007;52:2668–82.

[3] Secanell M, Karan K, Suleman A, Djilali N. Multi-variable optimization of PEMFC cathodes using an agglomerate model. Electrochim Acta 2007;52:6318–37.

[4] Harvey D, Pharoah JG, Karan K. A comparison of different approaches to modelling the PEMFC catalyst layer. J Power Sources 2008;179:209–19.

[5] Kamarajugadda S, Mazumder S. Numerical investigation of the effect of cathode catalyst layer structure and composition on polymer electrolyte membrane fuel cell performance. J Power Sources 2008;183:629–42.

[6] Rao RM, Bhattacharyya D, Rengaswamy R, Choudhury SR. A two-dimensional steady state model including the effect of liquid water for a PEM fuel cell cathode. J Power Sources 2007; 173:375–93.

[7] Siegel NP, Ellis MW, Nelson DJ, von Spakovsky MR. Single domain PEMFC model based on agglomerate catalyst geometry. J Power Sources 2003;115:81–9.

[8] Eikerling M, Kornyshev AA. Modelling the performance of the cathode catalyst layer of polymer electrolyte fuel cells. J Electroanal Chem 1998;453:89–106.

[9] Eikerling M. Water management in cathode catalyst layers of PEM fuel cells: a structure-based model. J Electrochem Soc 2006;153:E58–70.

[10] Liu J, Eikerling M. Model of cathode catalyst layers for polymer electrolyte fuel cells: the role of porous structure and water accumulation. Electrochim Acta 2008;53:4435–46.

[11] Soboleva T, Zhao X, Malek K, Xie Z, Navessin T, Holdcroft S. On the micro-, meso-, and macroporous structures of polymer electrolyte membrane fuel cell catalyst layers. ACS Appl Mater Interf 2010;2:375–84.

[12] Ceballos L, Prat M. Invasion percolation with inlet multiple injections and the water management problem in proton exchange membrane fuel cells. J Power Sources 2010;195: 825–8.

[13] Ceballos L, Prat M, Duru P. Slow invasion of a nonwetting fluid from multiple inlet sources in a thin porous layer. Phys Rev E 2011;84:056311.

[14] Gostick JT, Ioannidis MA, Fowler MW, Pritzker MD. Pore network modeling of fibrous gas diffusion layers for polymer electrolyte membrane fuel cells. J Power Sources 2007;173: 277–90.

[15] Sinha PK, Wang C-Y. Liquid water transport in a mixed-wet gas diffusion layer of a polymer electrolyte fuel cell. Chem Eng Sci 2008;63:1081–91.

[16] Hinebaugh J, Bazylak A. Condensation in PEM fuel cell gas diffusion layers: a pore network modeling approach. J Electrochem Soc 2010;157:B1382–90.

[17] Pulloor Kuttanikkad S, Prat M, Pauchet J. Pore-network simulations of two-phase flow in a thin porous layer of mixed wettability: application to water transport in gas diffusion layers of proton exchange membrane fuel cells. J Power Sources 2011;196:1145–55.

[18] Chapuis O, Prat M. Influence of wettability conditions on slow evaporation in two-dimensional porous media. Phys Rev E 2007;75:046311.

[19] Chapuis O, Prat M, Quintard M, Chane-Kane E, Guillot O, Mayer N. Two-phase flow and evaporation in model fibrous media: application to the gas diffusion layer of PEM fuel cells. J Power Sources 2008;178:258–68.

[20] El Hannach M, Pauchet J, Prat M. Pore network modeling: application to multiphase transport inside the cathode catalyst layer of proton exchange membrane fuel cell. Electrochim Acta 2011;56:10796–808.

[21] Wu R, Liao Q, Zhu X, Wang H. Pore network modeling of cathode catalyst layer of proton exchange membrane fuel cell. Int J Hydrogen Energy 2012;37:11255–67.

[22] Blunt MJ. Physically-based network modeling of multiphase flow in intermediate-wet porous media. J Petrol Sci Eng 1998; 20:117.

[23] Young JB, Todd B. Modelling of multi-component gas flows in capillaries and porous solids. Int J Heat Mass Transfer 2005; 48:5338–53.

[24] Schrage RW. A theoretical study of interphase mass transfer. New York: Columbia Univ. Press; 1953 [chapter 3].

[25] Siboni S, Della Volpe C. Some mathematical aspects of the Kelvin equation. Comput Math Appl 2008;55:51–65.

[26] Paul DK, Fraser A, Karan K. Towards the understanding of proton conduction mechanism in PEMFC catalyst layer: conductivity of adsorbed Nafion® films. Electrochem Commun 2011;13:774–7.

[27] Mann RF, Amphlett JC, Peppley BA, Thurgood CP. Application of Butler–Volmer equations in the modelling of activation polarization for PEM fuel cells. J Power Sources 2006;161:775–81.

[28] Bruggeman DAG. Berechnung verschiedener physikalischer Konstanten von heterogenen Substanzen. Ann Phys (Leipzig) 1935;24:636–79.

[29] Saad Y, Schultz MH. GMRES: a generalized minimal residual algorithm for solving nonsymmetric linear systems. SIAM J Sci Stat Comput 1986;7:856–69.

[30] Obut S, Alper E. Numerical assessment of dependence of polymer electrolyte membrane fuel cell performance on cathode catalyst layer parameters. J Power Sources 2011;196: 1920–31.

[31] Chaparro AM, Martin AJ, Folgado MA, Gallardo B, Daza L. Comparative analysis of the electroactive area of Pt/C PEMFC electrodes in liquid and solid polymer contact by underpotential hydrogen adsorption/desorption. Int J Hydrogen Energy 2009;34:4838–46.

[32] Sadeghi E, Djilali N, Bahrami M. Effective thermal conductivity and thermal contact resistance of gas diffusion layers in proton exchange membrane fuel cells. Part 2: hysteresis effect under cyclic compressive load. J Power Sources 2010;195:8104–9.